Chapter 4

IMAGING OF OCULAR AND ADNEXAL TRAUMA

JEFFREY P. BLICE, MD*

*Commander, Medical Corps, US Navy, Department of Ophthalmology, National Naval Medical Center, 8901 Wisconsin Avenue, Bethesda, Maryland 20889-5600

INTRODUCTION

Various imaging modalities exist to aid in the initial and subsequent evaluation of trauma involving the eye and orbit. However, the best imaging modality for the initial evaluation of eye trauma remains indirect ophthalmoscopy. In the first hours after a severe injury, the first examiner can obtain information with a level of detail that no other imaging method can provide. Although the early view may not always be the best one, often the first look into a traumatized eye is the only look.

Standard roentgenography, computed tomography (CT), magnetic resonance imaging (MRI), and ultrasonography all have their strengths and weaknesses. They can be useful adjuncts in the management of globe ruptures, intraocular foreign bodies (IOFBs), and facial and skull fractures.

Before beginning the discussion of available imaging methods, a brief review of orbital anatomy is in order. The orbit is pyramidal in shape, with the base oriented anteriorly and the apex posteriorly. The orbital walls consist of seven bones: the maxilla, zygoma, sphenoid, palatine, ethmoid, lacrimal, and frontal. The roof of the orbit is composed mainly of the frontal bone, with a small contribution from the sphenoid bone. Laterally, the zygoma and greater wing of the sphenoid provide the major component of the wall. Both the lateral and superior walls of the orbit are strong, but the inferior and medial walls have thinner bones and are more likely to be damaged from trauma. Inferiorly, the zygoma and thin roof of the maxilla form the major portion of the floor, and the palatine bone contributes posteriorly. The medial wall is formed from the frontal (superiorly), the sphenoid (posteriorly), the lacrimal (inferiorly and anteriorly), and the thin-walled ethmoid (centrally). The thin walls of the maxilla and ethmoid make these bones particularly susceptible to trauma from compression of the orbital contents or transmitted force applied to the orbital rim.

The optic canal is formed entirely from the lesser wing of the sphenoid. A traumatic injury resulting in dislocated bone fragments from the sphenoid can impinge on the optic nerve, resulting in a neuropathy.

IMAGING MODALITIES

Plain Skull Films

Although largely replaced now by CT scans, plain skull films (ie, roentgenography) can still provide useful information in the evaluation of traumatic injuries. It is likely that CT will not be easily accessible in a deployed medical unit; consequently, plain films of the skull may be the only imaging method available. The occipitofrontal, lateral, occipitooral, and oblique are the standard projections used to evaluate the orbit.

The occipitofrontal view, also called Caldwell's view or the anteroposterior (AP) view, provides a view of the size and shape of the orbit, the orbit floor, zygomaticofrontal suture, and lamina papyracea. The lateral view demonstrates the sella turcica, anterior and posterior clinoids, anterior and posterior walls of the frontal sinus, sphenoid sinus, and nasopharyngeal soft tissues. The occipitooral, or Waters's, view provides the best projection of the maxillary antra and inferior orbital rim. Oblique views are used to assess the shape and diameter of the optic canal, which has a normal range from 4.4 to 6.0 mm in diameter (Table 4-1).[1]

Plain films are relatively inexpensive and almost universally available; soft-tissue definition, however, is poor. Localization of foreign bodies (FBs) is unreliable without more-involved methods of imaging. Specifically, suturing a limbal ring to the eye and repeating AP and lateral views allow a radiologist to chart the position of an FB within the globe.[2] In instances of multiple radiopaque FBs, plain films permit a rapid assessment of the number and shape of the objects.

Computed Tomography

A CT image is a mathematical reconstruction of data obtained from multiple radiographic projections of an object. The basic principle of the CT scan involves an X-ray source and an array of detectors mounted in a gantry. The beam is projected through the object of interest, with the array of detectors measuring the attenuation of the beam. The X-ray source is then moved and the process repeated. The multiple projections are summed and converted to shades of gray, producing the CT image. The patient is then moved the thickness of the image slice, and the process is repeated for the next image.

The relative attenuation of the beam is expressed as Hounsfield units (HU), named in honor of the inventor of CT scanning. Water has a value of 0 HU, air a value of –1,000 HU, and dense bone a value of +1,000 HU (Table 4-2). An object with an HU

TABLE 4-1

APPROPRIATE PLAIN FILM ROENTGENOGRAMS FOR EYE IMAGING

View	Structures Demonstrated
Anteroposterior (AP) (or Caldwell's)	Size and shape of the orbits Superior orbital fissure Lamina papyracea Frontal and ethmoid sinuses Zygomaticofrontal suture
Occcipitooral (or Waters's)	Maxillary antra Orbital roof Inferior orbital rim Zygomatic bone and arch
Lateral	Sella turcica Clinoid processes Clivus Walls of frontal sinus Sphenoid sinus
Oblique (or optic foramen)	Optic foramen Superior orbital fissure Lacrimal fossa Ethmoid air cells

Adapted with permission from Weber AL. Imaging techniques and normal radiographic anatomy. In: Albert DM, ed. *Principles and Practice of Ophthalmology.* Vol 5. Philadelphia, Pa: WB Saunders Company; 1994: 3505.

TABLE 4-2

COMPUTED TOMOGRAPHY ATTENUATION COEFFICIENTS FOR VARIOUS FOREIGN BODIES

Foreign Body	Attenuation Coefficient (HU)*
Air	–1,000
Aluminum	1,150
Bakelite	400
Brick	400
Ceramic	2,000
Chromium	6,000
Copper	1,600
Glass	1,400–2,800
Graphite	260
Iron	3,800–20,600
Lead	11,600
Mica	25
Porcelain	600
Solder	6,500
Stone	500
Water	0
Wood	5

*Hounsfield units
Adapted with permission from Gunenc U, Maden A, Kaynak S, Pirnar T. Magnetic resonance imaging and computed tomography in the detection and localization of intraocular foreign bodies. *Doc Ophthalmol.* 1992;81:371.

value of 0 appears isodense with water, and objects with higher HU values appear brighter—bone, for example. Adjustment of the grayscale window can highlight bony anatomy over soft-tissue anatomy. Modern CT scanners have a fixed array of detectors with a rapidly moving source, permitting decreased scan times and higher spatial resolutions. Relatively new scanners move the patient through the gantry continuously at the rate of one slice thickness per revolution of the X-ray source. This is called a helical or spiral CT; scan time is shortened further, and patient movement artifact is limited.[3–5]

CT scans of the eye and orbit can produce axial or coronal images. The plane of these images and representative slices for an axial and coronal section are demonstrated in Figures 4-1 and 4-2. Slices in the axial plane are usually 1 to 3 mm in thickness when specifically imaging the orbit. Protocols for scanning orbits may vary from institution to institution; if necessary, specify thin sections (1.5 or 3.0 mm) when ordering the study. Axial images provide good cross-sectional anatomical views of the orbit, globe, and skull. Localization of structures in and around the globe is immensely improved over plain films, and the improved view of bony anatomy provides an excellent view of the optic canal.

Coronal images can be reconstructed from the data obtained during an axial scan; however, direct coronal scans offer improved resolution. These sections are usually obtained by placing the patient's neck in a slightly extended position while moving through the gantry. The plane of these images may not be truly coronal but oblique to the true plane. Adjusting the head position can avoid "spray" artifacts from dental work.

Software is now available for reconstruction of three-dimensional images of the entire skull. Although not useful in every case, these images can be useful in the reconstruction of severe orbital trauma.

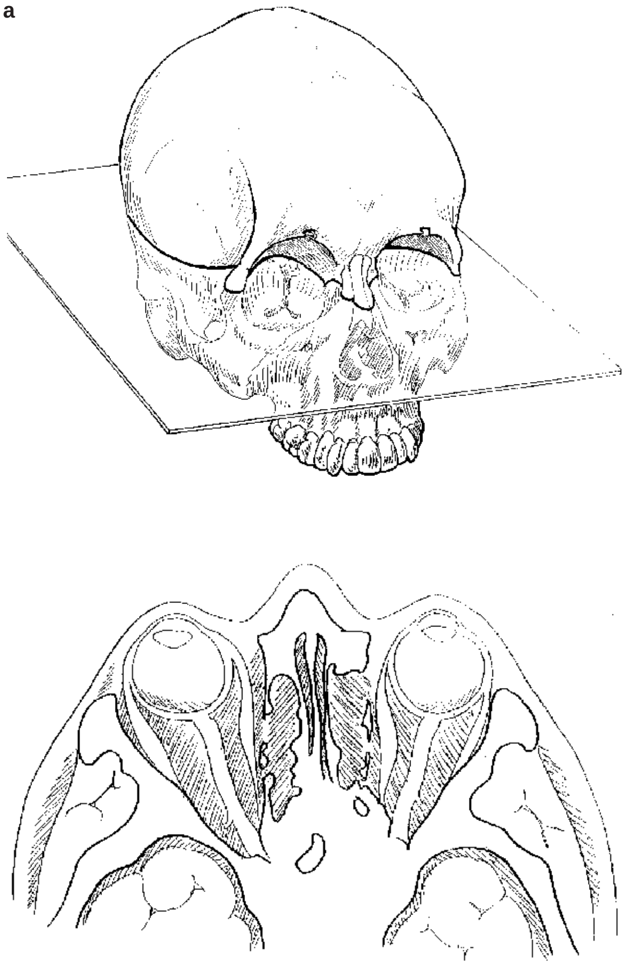

Fig. 4-1. (**a**) A diagram of a skull with the axial plane of the section demonstrated through the midorbit. (**b**) The approximate appearance of a computed tomography section corresponding to the plane of the section in view (a). Fractures of the roof and floor are in the same plane as an axial section and are difficult to detect in these views. Drawings prepared for this textbook by Gary Wind, MD, Uniformed Services University of the Health Sciences, Bethesda, Md.

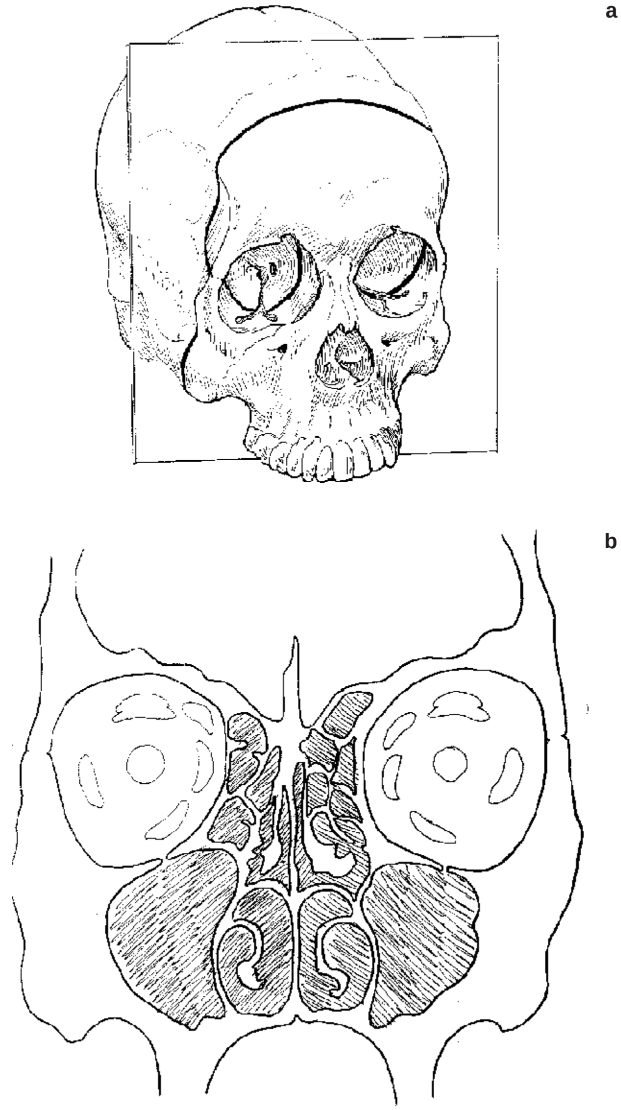

Fig. 4-2. (**a**) A diagram of skull with the coronal plane of a section demonstrated through the midorbit. (**b**) The approximate appearance of a computed tomography section corresponding to the plane of the section in view (a). Fractures through any of the walls of the orbit are more easily seen in these sections. Reconstructed images have suboptimal resolution, so direct coronal sections should be obtained if possible. Drawings prepared for this textbook by Gary Wind, MD, Uniformed Services University of the Health Sciences, Bethesda, Md.

Magnetic Resonance Imaging

A detailed discussion of the theory behind MRI scanning is beyond the scope of this chapter; however, knowledge of the basic principles is useful for understanding the application of this imaging modality in ocular and orbital trauma.

The general principle of MRI is that the nuclei of certain atoms become aligned when placed in a magnetic field. A pulse of radio frequency (RF) energy can be applied to these nuclei, resulting in a shift of the net magnetic vector of 90° or 180°. This process involves the absorption of RF energy. The duration and energy of the pulse affect the hydrogen atoms in human tissue. After the RF pulse is terminated, the nuclei will "relax," or realign a

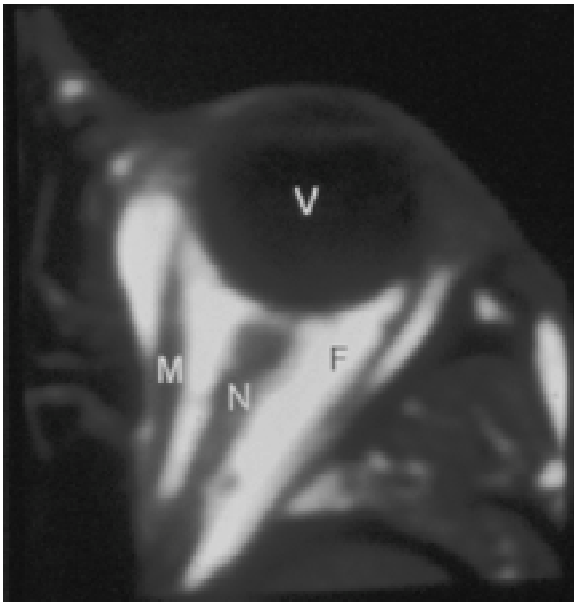

b

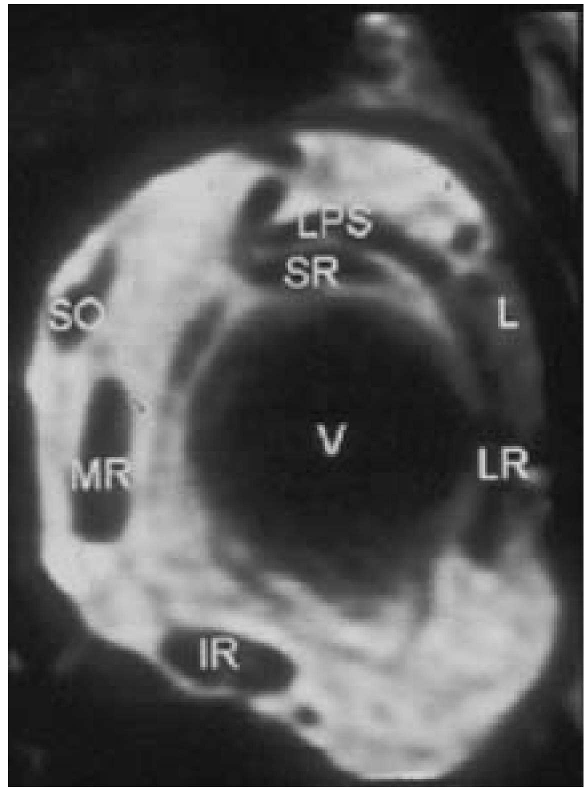

Fig. 4-3. Magnetic resonance imaging scans of a normal orbit, T1-weighted images. (**a**) In this axial section, the vitreous (V) appears dark. Extraocular muscles (M) and optic nerve (N) appear dark. Fat (F) produces a high signal and appears bright. Fat-suppression protocols improve the quality of images by compensating for the increased signal produced by the orbital fat. (**b**) This coronal section provides an excellent view of the vitreous (V) and the lateral rectus (LR), inferior rectus (IR), medial rectus (MR), superior oblique (SO), levator palpebrae superioris (LPS), and superior rectus (SR) muscles. The lacrimal gland (L) can be seen in the lateral orbit; the signal is similar to other soft tissues in the orbit.

themselves with the magnetic field, and they emit RF energy that can be measured with an antenna. This antenna can be intrinsic to the MRI scanner or it can be a surface coil placed over the orbit, which improves image resolution. Gadolinium, a paramagnetic contrast agent, can be given intravenously to enhance vascular anatomy and orbital pathology.

Through manipulation of the various RF pulses and measurements of the resulting emitted energy, different images can be constructed. The most common of these images are the T1-weighted, T2-weighted, and proton density–weighted. The parameters used to produce a T1-weighted image result in a characteristic appearance of ocular structures (Figure 4-3). Vitreous and cerebrospinal fluid appear dark, muscle and nerve appear equally dark with the white matter of the central nervous system, and fat appears very bright. The great contrast between these structures provides the best anatomical detail of the orbit. However, a small orbital lesion may be hidden by the strong signal produced by orbital fat. Melanin and blood appear bright on a T1-weighted image as well; consequently, subretinal hemorrhage and ocular melanomas can be detected on these images.

On T2-weighted images, vitreous and cerebrospinal fluid appear bright, and fat appears dark (Figure 4-4). The scanning times are longer and, consequently, spatial resolution suffers, although tumor infiltration, edema, and demyelination are better demonstrated. Proton density–weighted images reflect the number of MRI-visible protons in a given unit volume. The proton density of the tissues in and around the orbit differs minimally, causing tissue contrast to be relatively low and limiting the usefulness of these images.

Fat-suppression protocols have been developed to decrease the signal intensity of orbital fat, which, in combination with gadolinium, can improve visualization of the optic nerve and enhancing lesions. The views produced with an MRI scan are similar to those produced by CT. There are axial and coronal images, and sagittal images are also produced. Unlike CT, though, the coronal and sagittal images are always reconstructions.

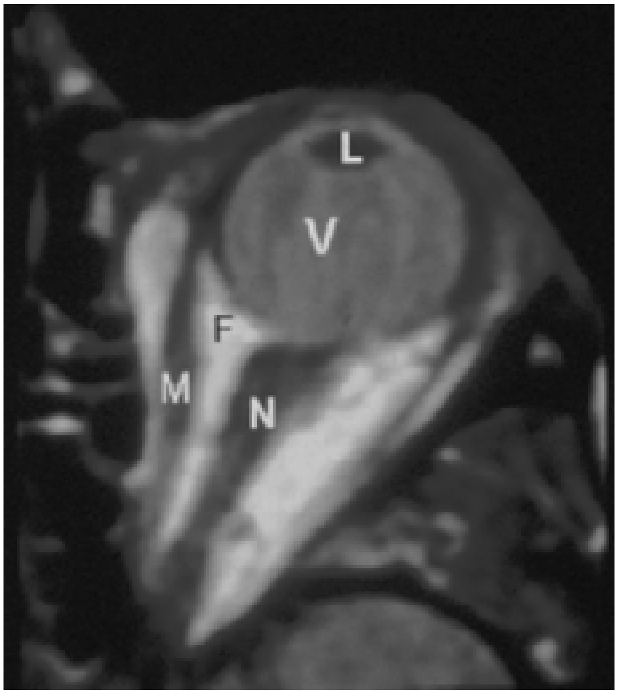

Fig. 4-4. Magnetic resonance imaging scans of a normal orbit, T2-weighted images. The view of the orbit in this axial section is similar to that in Figure 4-3a except that the image is T2-weighted. The vitreous (V) in this case appears relatively bright. The lens (L) produces a low signal and can be seen in the anterior segment. The extraocular muscles (M), optic nerve (N), and fat (F) all appear dark. Bone is poorly demonstrated in all views of the magnetic resonance imaging scan.

Ultrasonography

Ocular ultrasonography is a useful diagnostic tool when media opacities preclude using standard means to view the ocular structures and is especially helpful when used in conjunction with other imaging modalities. Ultrasonography was initially developed in the late 1950s to evaluate intraocular tumors. Over the ensuing decades, improvements in technology have made ultrasonography a routine diagnostic tool.

Ultrasound is defined as sound frequency greater than 20 kHz. Medical applications use ultrasound frequencies in the 2- to 50-MHz range. Lower frequencies provide good penetration of tissue but sacrifice resolution. Higher frequencies provide increased resolution but at the price of tissue penetration. Transducers with a frequency of 7.5 to 12.0 MHz have low penetration, approximately 6 cm at 7.5 MHz with resolution of 0.1 mm at 8 MHz.[6] Higher-frequency transducers operating in the 50-mHz range produce high-resolution images; however, they concentrate on small portions of the anterior segment or anterior structures of the posterior segment. This equipment is relatively expensive and, although useful in certain circumstances, is not readily available at all institutions.[7,8]

The instrument itself consists of a handheld transducer containing a piezoelectric crystal or synthetic ceramic. When an electrical potential is applied across the crystal, the crystal is mechanically deformed, and an ultrasonic pulse is emitted. The echoes produced are received by the transducer and converted back into electrical impulses. These impulses are amplified and converted into a video display.[6] The sound wave produced by the transducer can be reflected, refracted, or absorbed. Different tissues in the eye and orbit have different densities and, therefore, different acoustical impedance. At the anatomical boundaries of these tissues there is a mismatch of acoustical impedance, resulting in reflection and refraction of the sound wave. The intensity of the reflection, or echo, depends on the magnitude of the acoustical impedance mismatch. The intensity of the echo also depends on the angle at which a sound wave reaches an interface: a perpendicular wave is fully reflected, but an oblique wave is only partially reflected. In addition, the shape, size, and regularity of an object can influence the strength of an echo.[9]

The echoes can be displayed in two formats: amplitude (A) or brightness (B) modulation. Amplitude modulation, or A-scan, displays the intensity of the echo as a vertical spike plotted against the echo's time delay, which is equivalent to the distance from the transducer. This mode is useful in measurements of intraocular length for intraocular lens calculations and in diagnosis of intraocular and intraorbital tumors. The usefulness of the A-scan in the evaluation of ocular trauma is limited at best.

Brightness modulation, or B-scan, displays a two-dimensional representation of the eye. The intensity of an echo is proportional to the brightness of a dot on the display. The B-scan is a dynamic examination providing real-time, two-dimensional images of the ocular and orbital structures. Although photographic static images of the B-scan are obtained for a permanent record, the kinetic nature of the study can provide more information than can be documented by a photograph. Therefore, the ability to perform a B-scan can be an invaluable tool in the diagnosis and evaluation of ocular trauma.

Of the imaging modalities discussed, ultrasound is the only one in which the ophthalmologist controls the access to and quality of the study.

SPECIFIC TRAUMATIC INJURIES AND IMAGING

Intraorbital and Intraocular Foreign Bodies

The detection and localization of intraocular and intraorbital FBs are important and potentially difficult tasks in the management of ocular trauma. All the modalities discussed are potentially useful in the detection of FBs and are particularly useful when applied together to obtain a complete picture.

Although almost universally replaced by the CT scan, plain films of the skull, as mentioned earlier, are useful for rapid evaluation of the presence, size, number, and shape of FBs in and around the eye (Figures 4-5 and 4-6). The poor localization of the objects, however, makes the use of other methods necessary. B-scan ultrasonography is a very useful method for determining the presence or absence of FBs that lie within or near the globe.

Ultrasonography can detect an object independent of its radiopacity and can differentiate between intraocular and extraocular objects when they are located near the sclera. Usually, an IOFB will appear as a reflective object either in midvitreous or lying near the retina (Figure 4-7). An example of an extraocular object (a BB) lying next to the medial rectus is shown in Figure 4-8. The ultrasound artifacts of acoustical shadowing (see Figure 4-7) and reverberations (see Figure 4-8) aid in the detection of the FB, and when an object passes through the vitreous, a track can often be seen (Figure 4-9). Air bubbles within the vitreous, which may appear in the globe as a result of trauma, may resemble an FB. Air tends to be more uniform in reflectivity, maintaining its shape and reflectivity from different angles, but the reflection off an FB will only be high from waves that strike perpendicular to its surface.

The use of ultrasound biomicroscopy for the detection and localization of occult FBs was reported in 1999.[10] Ultrasound biomicroscopy is a useful adjunct in the detection and localization of small nonmetallic objects, predominantly in the anterior segment or the anterior, posterior segment (Figure 4-10). Unfortunately, this equipment is not readily available at most facilities.

Although plain films and ultrasonography together may provide enough information to determine the general location of an FB, a CT scan is the standard of care in the evaluation of these injuries. In fact, in cases in which an FB cannot be seen but a high index of suspicion exists, a CT should be obtained to rule out a foreign object.

Without question, CT scanning is useful in de-

a

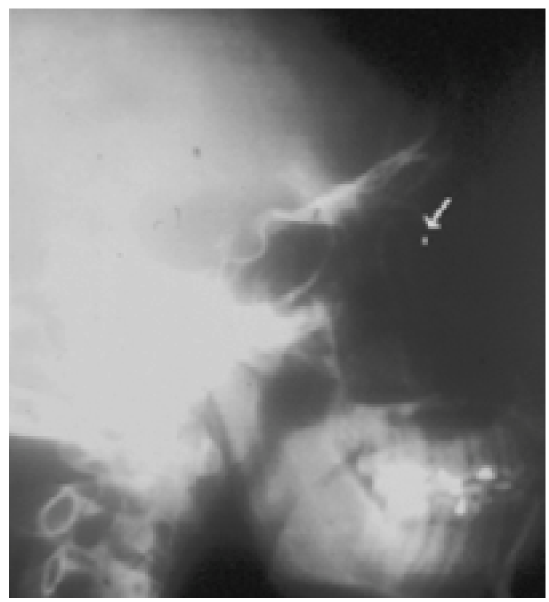

b

Fig. 4-5. (**a**) This is a plain radiograph, occipitooral (Waters's) view, of a patient who was hammering metal on metal and noticed a sudden decrease in vision. On presentation, a self-sealing corneal laceration was present, as well as a developing cataract. The arrow demonstrates a radiopaque foreign body (FB) somewhere in the orbit. (**b**) Lateral plain film of the same patient demonstrates the FB (indicated by arrow) present in the anterior orbit. Although multiple views help localize an FB on plain films, definitive localization of this FB was provided by indirect ophthalmoscopy by the initial examiner. The FB was seen lying nasal to the nerve. Subsequent computed tomography and ultrasonography confirmed an intraocular FB in the vicinity described by the initial exam.

Fig. 4-6. Plain radiograph, occipitofrontal view, reveals a relatively large radiodense object, which can be seen in the orbit. Radiograph: Courtesy of William Benson, MD, Philadelphia, Pa.

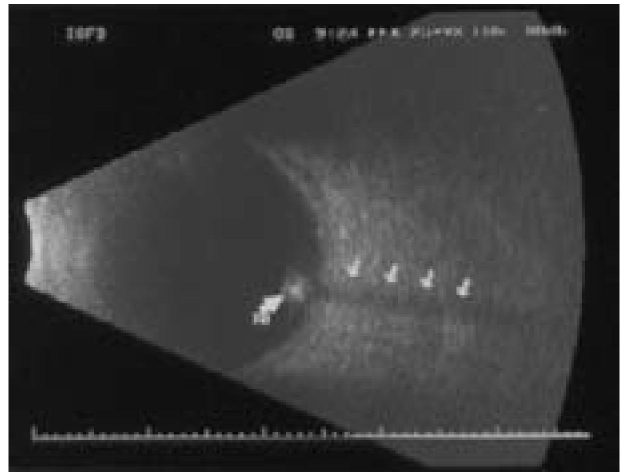

Fig. 4-7. A brightness modulation (B-scan) ultrasound study of an intraocular foreign body (IOFB) reveals a highly reflective FB just anterior to the retina; acoustic shadowing is also seen, as indicated by small arrows. The ultrasound characteristics of an FB depend on the nature and shape of the object. The appearance can also be affected by the angle at which the sound wave strikes the object. When the acoustic wave strikes the object perpendicularly and maximum reflection is obtained, shadowing occurs behind the object. If the angle of incidence is not perpendicular or the surface of the FB is poorly reflective, shadowing may not be seen. Sonogram: Courtesy of Elizabeth L. Affel, MS, RDMS, Philadelphia, Pa.

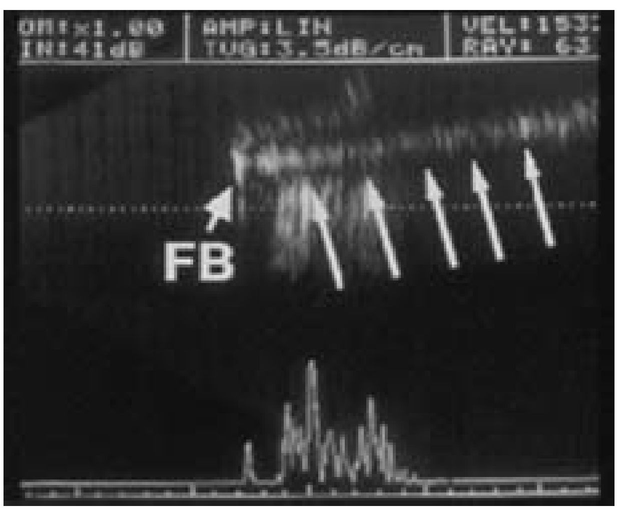

Fig. 4-8. A patient was shot in the eye with a BB gun; however, no clinical evidence of a ruptured globe was found. A brightness modulation (B-scan) ultrasound examination revealed a highly reflective foreign body (FB) with multiple reverberations, indicated by small arrows. The reverberations seen here are classic for a BB pellet. Although other foreign bodies produce reverberations, the spherical shape of this object produces this unique appearance. The B-scan does not demonstrate a vitreous cavity because the object is lying outside the globe near the medial rectus muscle. This position was confirmed on exploration of the orbit and removal of the object.

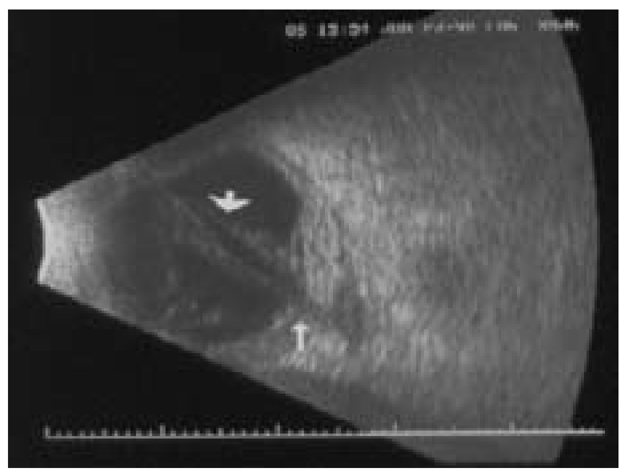

Fig. 4-9. A brightness modulation (B-scan) ultrasound examination of patient with a posterior rupture of the globe. When a foreign body passes through the vitreous cavity, an apparent track through the vitreous can be seen, as demonstrated by the short arrow. In this case, the object passed through the posterior sclera at a point indicated by the longer arrow. The B-scan does not demonstrate the foreign body directly but does provide useful information about the status of the intraocular structures in a circumstance in which the view is likely to be poor. Sonogram: Courtesy of Elizabeth L. Affel, MS, RDMS, Philadelphia, Pa.

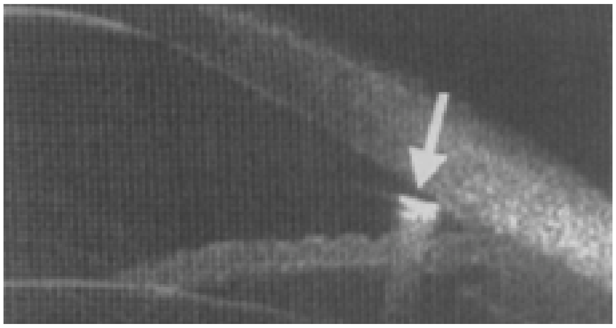

Fig. 4-10. Ultrasound biomicroscopy revealing an occult foreign body. Although ultrasound biomicroscopy requires specialized equipment, the exquisite detail of anterior segment structures makes it an excellent tool for detecting small, otherwise poorly visualized foreign objects. Reproduced from Deramo VA, Shah GK, Baumal CR, Fineman MS, Correa Zm, Benson WE. Ultrasound biomicroscopy as a tool for detecting and localizing occult foreign bodies after ocular trauma. *Ophthalmology.* 1999;106:303.

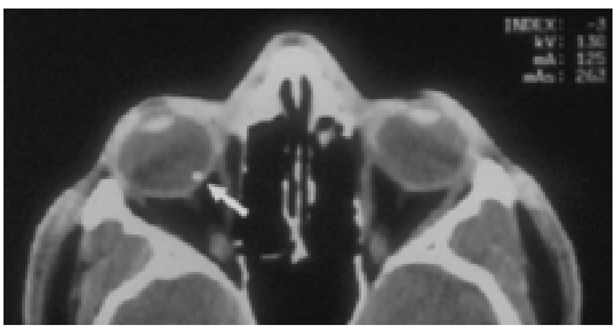

Fig. 4-12. Another computed tomography scan, axial section, from the same patient as in Figure 4-9, at the level of midglobe. The lens is clearly visible on both sides. A single radiodense object, indicated by the arrow, is seen within the globe. The object appears to be located adjacent to the nerve on the nasal retina. The position of the object was confirmed by indirect ophthalmoscopy to be one disc diameter nasal to the optic disc.

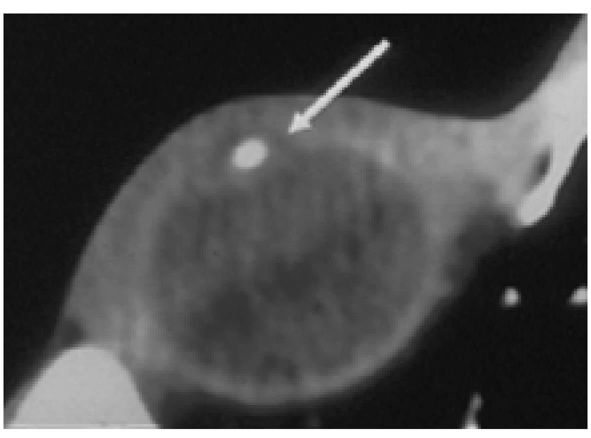

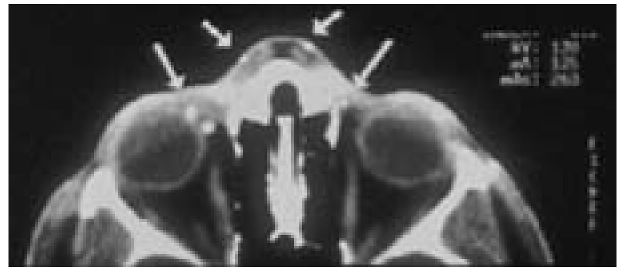

Fig. 4-11. A patient involved in ordnance disposal was injured by an explosion and presented with multiple facial lacerations and visual symptoms in the right eye. This computed tomography scan, axial section, through the orbit reveals multiple radiodense objects in the superficial tissues of the face and within the orbits bilaterally. Note the two objects lying outside the medial aspect of the left globe.

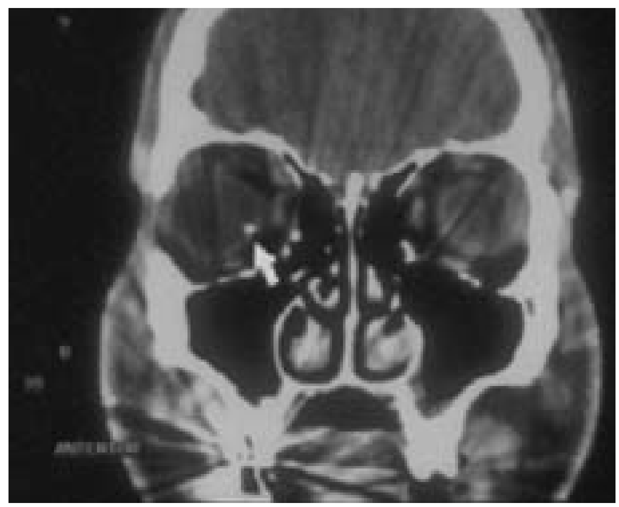

Fig. 4-13. This computed tomography scan, direct coronal section, of the same patient whose plain films are seen in Figure 4-5, demonstrates the same radiodense foreign body (FB), indicated by an arrow, in the globe on the nasal aspect. The combination of the coronal and axial sections provided an accurate determination of the position of the FB. Surgical removal of the FB was required; a metallic FB was located on the nasal retina. Spray artifact from dental work also can be seen.

Fig. 4-14. While training on the rifle range, this patient noticed a sudden pain in his eye after a shell casing was discharged from a nearby rifle and struck the concrete beside him. Anterior segment examination revealed an area of fibrin in the inferior angle, but no foreign body could be confirmed. The computed tomography enlarged view of axial section seen here demonstrated a single, radiodense foreign body in the anterior segment, indicated by the arrow. On exploration, a small limbal laceration was noted and a 1-mm piece of mineral material was located in the anterior chamber.

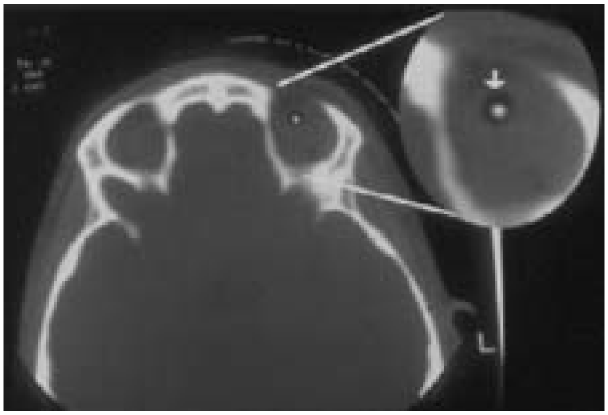

Fig. 4-15. A computed tomography scan, axial section, with enlargement of orbit (inset) of a patient in whom a pencil had passed through the eyelid and into the orbit and brain. The relative radiopacity of the graphite is clearly seen, as well as the relative radiolucency of the surrounding wood. This demonstrates how a wooden foreign body within the orbit may escape detection; a magnetic resonance imaging scan might well provide more information in cases like this. Computed tomography scan: Courtesy of Allen Thach, MD, Phoenix, Ariz.

tecting FBs made of glass, metal, or mineral (Figures 4-11 to 4-14). Lead, iron, solder, and chromium have relatively high attenuation coefficients; glass and stone have lower coefficients but still appear relatively bright. Wood is almost isodense with water and may be difficult to distinguish from the surrounding soft tissue (Figure 4-15). The size and volume of these objects are also factors in their detection.[11,12] Steel objects with a volume as small as 0.048 mm^3 are detectable by CT scan, although steel objects with a volume greater than 0.06 mm^3 were detected with a greater sensitivity in one experimental model.[4]

Helical or spiral CT scans present some benefits over conventional CT scanning, and the ability to detect steel IOFBs seems equivalent to that of conventional CT.[4] Scan times for the entire orbital volume can be as fast as 18 seconds, which will minimize motion artifact and reduce radiation exposure. Furthermore, unlike conventional CT, high-resolution coronal and sagittal images can be reconstructed from the axial scans, further limiting radiation exposure. Total exposure may be approximately one fourth that required for a conventional CT.[5] Helical CT may be ideal for patients with limited ability to cooperate or limited ability to position for conventional coronal CT scans.

Although excellent for the detection of high-density materials, CT is poor for organic matter of comparable size.[13,14] MRI has been suggested[15] as a reliable method to detect nonmetallic FBs (glass, plastic, or mineral), but the detection of organic matter may be much less reliable. A retrospective study[16] concluded that identification of foreign material in the orbit was possible in only about 50% of cases with the use of CT and MRI.

The potential danger of MRI in the face of a ferromagnetic FB in or outside the globe is clearly recognized. An intraocular magnetic object can move and grossly deform the globe[17] or move through the orbit, potentially causing a blinding injury.[18] A CT scan or plain film to exclude an iron or steel FB is a prerequisite for an MRI in the setting of an intraorbital or intraocular FB.

Orbital Fractures

Fractures of the orbital bones can result from direct trauma to the facial bones or compression of the orbital soft tissues, resulting in a blowout fracture of the orbit. Plain films of the skull are still used in emergency departments to screen for these fractures, and usually the telltale sign of an air–fluid level in the maxillary sinus prompts further radiographic evaluation. The definitive evaluation of bony anatomy provided by the CT scan is an integral part of the management of these injuries.

When an orbital fracture is suspected, a CT scan with both axial and direct coronal sections should be obtained. A section 1.5 mm to 3.0 mm in thickness is the usual protocol; very thin sections require a longer scan time, straining the resources of the radiologist, and the extra information obtained may not alter the management of the injury. The recent development of the helical CT may provide imaging options in patients with limited ability to cooperate or position for direct coronal sections. Three-dimensional reconstruction, which requires the manipulation of digital images with special software, may also be useful in the management of complex orbital fractures. Although three-dimensional imaging may not be useful to the general ophthalmologist, an orbital surgeon faced with a difficult reconstruction may find the information valuable. When considering these more-complex imaging options, we should consult a radiologist early in the process to ensure that the desired result is obtained most efficiently.

Fractures of the orbital walls are most easily seen on coronal sections. Irregularities in the contours of the medial or inferior orbital walls, as well as

Fig. 4-16. The patient is a young woman who was involved in a serious automobile accident, which resulted in multiple facial fractures. The arrows on this computed tomography scan, coronal view, demonstrate bilateral, commuted orbital floor fractures. Other fractures involving the ethmoid sinuses also can be seen. Note how spray artifact from dental work affects the overall quality of the image.

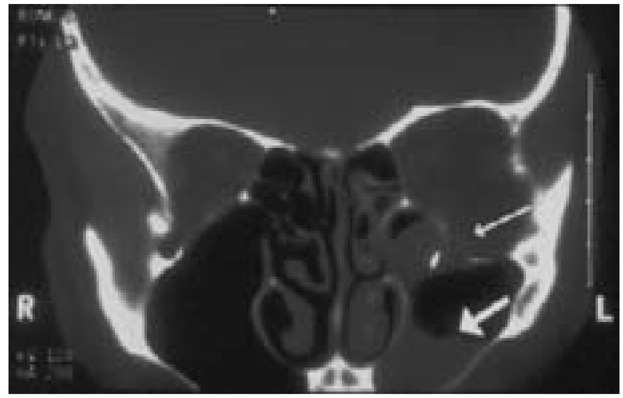

Fig. 4-17. This computed tomography scan, coronal view, is of a patient who sustained a direct blow to the face. The grayscale window is adjusted to highlight bone. The longer arrow demonstrates a fracture of the orbital floor, left orbit. Hemorrhage into the maxillary sinus causes opacification of the maxillary sinus and an air–fluid level, demonstrated by the shorter arrow.

opacification of the ethmoidal or maxillary sinuses, are the usual findings in blowout fractures of the orbit (Figures 4-16 and 4-17). Prolapse of orbital contents into the maxillary sinus or intraorbital emphysema may also be seen. Because entrapment of the inferior rectus is often at issue in these injuries, careful examination of sections through the muscle cone is required. An area of prolapsed orbital fat or hemorrhage into the sinus mucosa must be differentiated from a truly entrapped rectus muscle (Figure 4-18). Fractures of the lateral and superior orbital rims are less common but can impinge on the intraorbital contents (Figure 4-19).

Following the fracture from the point of initial detection and summing the thicknesses of the sections involved until the end of the fracture can yield an estimate of the size of the fracture. The involvement of neurovascular structures can also be assessed by examination of the infraorbital canal. A depression of the bony canal or groove will often correlate with infraorbital hypesthesia (Figure 4-20).

The optic nerve is subject to trauma from bony fragments impinging on it at or near the optic canal. Axial CT images can provide high-resolution images of the bony anatomy surrounding the nerve. If optic nerve damage is suspected, the possibility

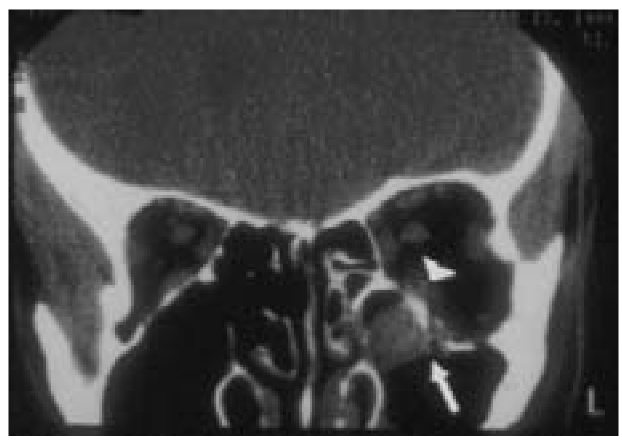

Fig. 4-18. The patient sustained head and facial trauma from a fall down a staircase. This computed tomography scan, coronal view, reveals an orbital floor fracture in the left orbit. The grayscale is adjusted to highlight the view of orbital soft tissues. A short arrow points directly to the inferior rectus muscle, which does not appear to be trapped in the fracture site; a mass of tissue is seen protruding at the fracture site (long arrow). On close examination, the mass appears inferior to the nondisplaced bone fragment; most likely, it represents a hemorrhage into the mucosa of the maxillary sinus, not a herniation of orbital fat. These findings are consistent with the unimpaired ocular motility of the patient.

a b

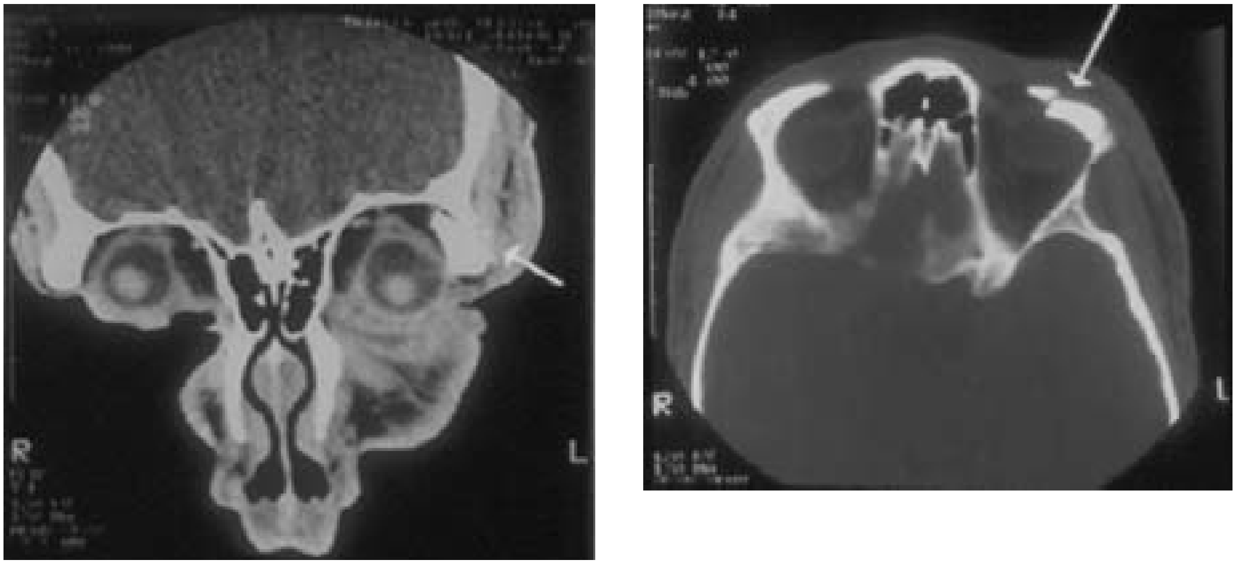

Fig. 4-19. (**a**) This computed tomography scan, coronal section, demonstrates an orbital fracture involving the zygomatic-frontal suture (arrow) with displacement of the bone fracture into the orbit. Associated soft-tissue swelling is also visible on the lateral aspect of the skull. The patient was unable to elevate the globe. (**b**) This computed tomography scan, axial section, of the same patient demonstrates bony fragments (indicated by arrow) impinging on the globe and interfering with supraduction. Computed tomography scans: Courtesy of Allen Thach, MD, Phoenix, Ariz.

Fig. 4-20. The patient sustained sports injury to the right orbit 6 months before this computed tomography study, coronal view, was done. The long arrow indicates a fracture of the right orbital floor involving the infraorbital canal. The depression of the canal is consistent with the infraorbital hypesthesia seen in these fractures. The absence of an air–fluid level and a clear picture of the displaced sinus mucosa (arrowhead) suggest that the injury is not acute.

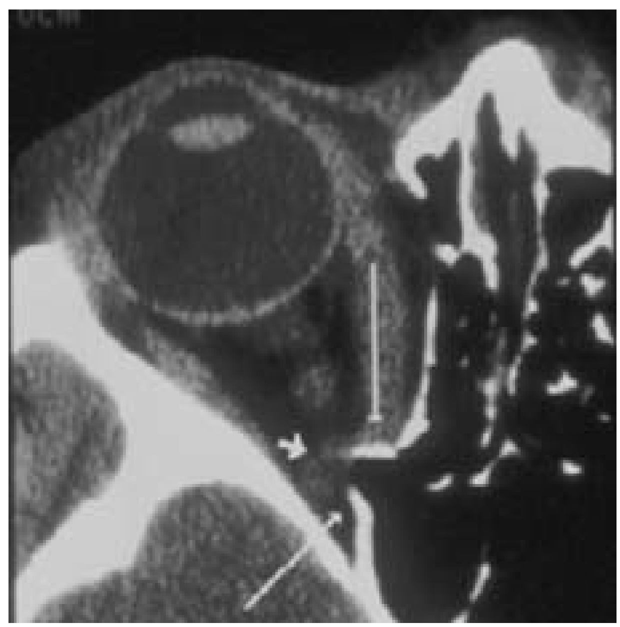

Fig. 4-21. A computed tomography scan, axial view, of a patient with multiple skull fractures and no light perception following a motor vehicle accident. Fragments of the sphenoid bone (long arrows) can be seen impinging on the optic nerve (short arrow). The axial section through the optic canal can provide valuable information when a traumatic injury from a bone fragment is suspected.

should be brought to the attention of the radiologist before the study is obtained to ensure adequate imaging of the nerve and surrounding bone. Early detection of bone fragments impinging on the nerve can provide an opportunity for treatment by decompression, or at least early detection can provide useful information to guide the treatment of the traumatized eye and aid in the formulation of a realistic prognosis (Figure 4-21). In any case, when visual loss seems out of proportion to findings on ophthalmoscopy, the possibility of traumatic optic neuropathy must be considered.

Blunt Ocular Trauma

The value of radiographic evaluation of the globe with CT is limited except in those incidents in which a nebulous history cannot exclude the presence of an FB. Although a CT scan may confirm a deformed globe in cases of occult ruptures, the findings on a CT scan are unlikely to precipitate or prevent an exploration of a bluntly traumatized eye. An eye that is suspected to have an occult rupture on clinical examination should be explored with or without supporting radiographic evidence.

Although MRI is of limited use in the general evaluation of ocular trauma, in specific instances it can be helpful. The exceptional images of orbital soft tissues provided by MRI can aid in the evaluation of trauma to the extraocular muscles. Figure 4-22 demonstrates a case involving blunt ocular trauma with an inability to infraduct the eye. CT was not able to demonstrate the injury to the inferior rectus muscle.

Ultrasonography, on the other hand, can be an invaluable tool in the evaluation of a bluntly traumatized eye with a poor or absent view of the posterior segment. Although extreme care must be exercised to avoid any pressure on the eye with a suspected rupture, an ultrasound examination can be performed to confirm a globe rupture and assess the status of the retina (see Figure 4-9). For a patient with a ruptured globe, B-scan is often the only source of information to guide postoperative care.

A dislocated lens or lens fragment, vitreous detachments, retinal tears, retinal detachments, and choroidal detachments are all complications of blunt ocular trauma that can be diagnosed by ultrasonography (Figures 4-23 to 4-26). CT and MRI are capable of imaging some, if not all, of the aforementioned entities; however, ultrasonography is a more economical and practical method for diagnosis and follow-up examinations. Because the quality of the examination is

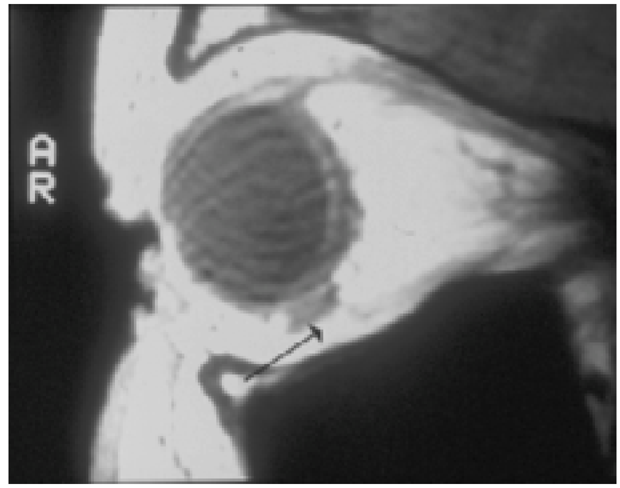

Fig. 4-22. A sagittal magnetic resonance imaging scan of an orbit, T1-weighted. This patient fell on a metal pipe, subsequently losing the ability to infraduct the eye. A computed tomography scan was not helpful in the evaluation of the problem; the magnetic resonance imaging scan, however, demonstrated a discontinuity in the inferior rectus muscle. Magnetic resonance imaging provides excellent images of the orbital soft tissues, especially the extraocular muscles; the arrow highlights the discontinuity in the inferior rectus. Adapted from Ward TP, Thach AB, Madigan WP, Berland JE. Magnetic resonance imaging in posttraumatic strabismus. *J Pediatr Ophthalmol Strabismus.* 1997;34:132.

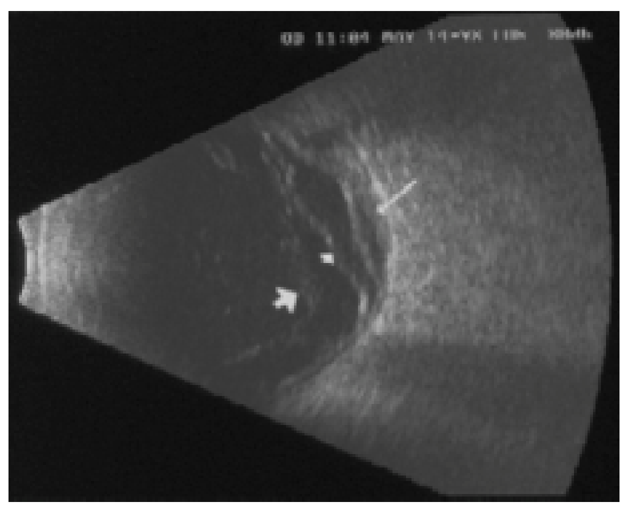

Fig. 4-23. High-quality ultrasound can provide information about the anatomical status of the intraocular structures when no view is possible. This brightness modulation (B-scan) ultrasound study demonstrates a posterior vitreous detachment (large arrow), a retinal detachment (smaller arrow), and a choroidal detachment (long arrow). Sonogram: Courtesy of Elizabeth L. Affel, MS, RDMS, Philadelphia, Pa.

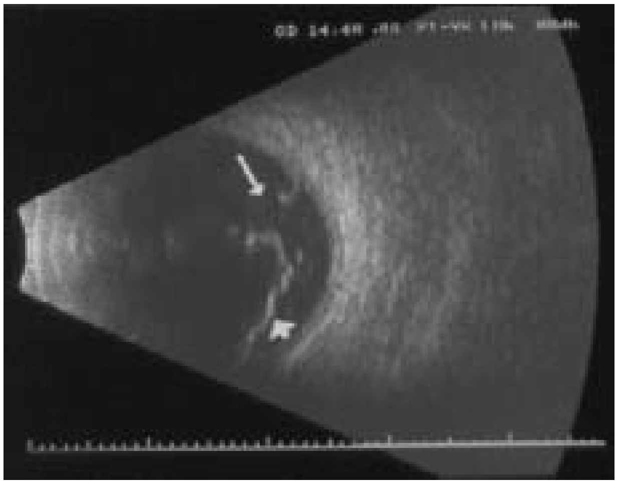

Fig. 4-24. In the hands of a skilled examiner, a high-quality ultrasound can demonstrate details usually only detectable on ophthalmoscopy. This brightness modulation (B-scan) ultrasound study demonstrates a retinal detachment, indicated by the small arrow, and the cause, a retinal tear demonstrated by the larger arrow. Sonogram: Courtesy of Elizabeth L. Affel, MS, RDMS, Philadelphia, Pa.

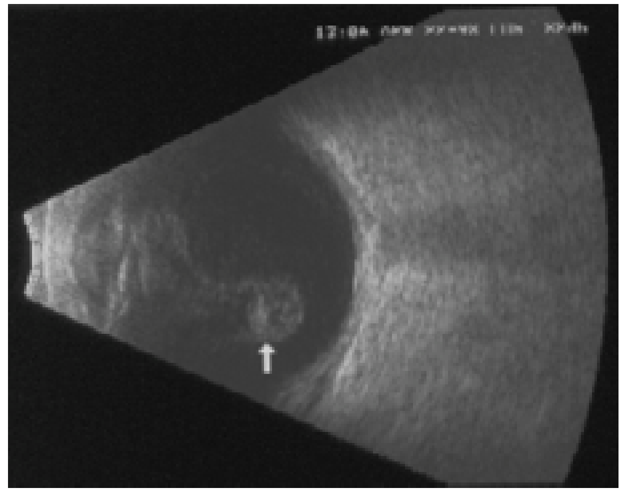

Fig. 4-25. A lens dislocated into the posterior segment (arrow) can easily be detected by brightness modulation (B-scan) ultrasonography. Sonogram: Courtesy of Elizabeth L. Affel, MS, RDMS, Philadelphia, Pa.

a

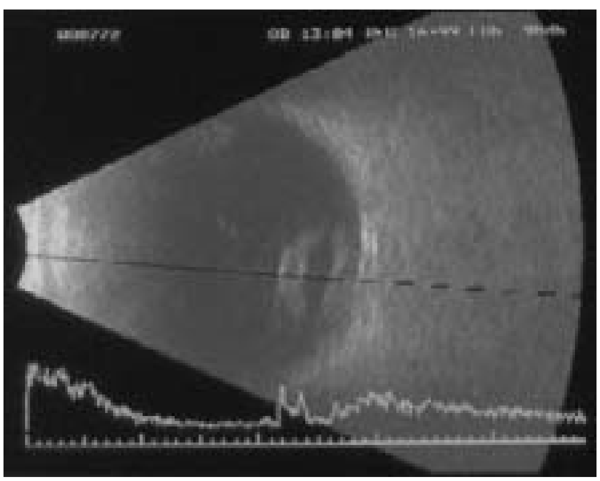

b

c

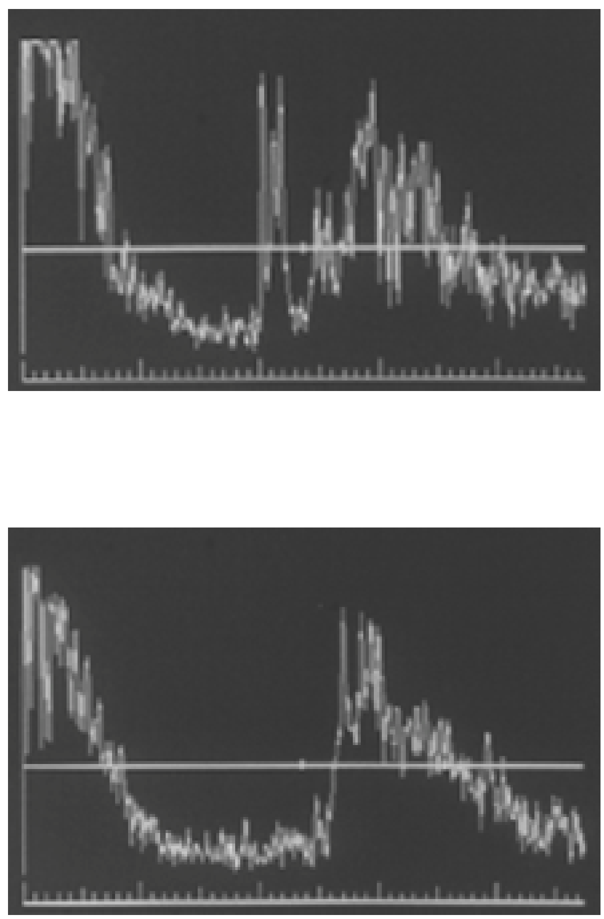

Fig. 4-26. (**a**) A brightness modulation (B-scan) ultrasound study of a patient with a remote history of ocular trauma. The dislocated native lens can be seen resting on the surface of the retina. (**b**) An amplitude modulation (A-scan) ultrasound study of the same patient demonstrates a peak at the position of the anterior surface of the dislocated lens. (**c**) An A-scan ultrasound study of a normal eye, in which echoes are plotted against time, reflecting the distance of the target from the probe. An absence of echoes is noted through the vitreous cavity until a sharp peak generated by the surface of the retina is encountered. In the hands of most ophthalmologists, for the detection and analysis of foreign bodies, the usefulness of A-scan ultrasonography is limited.

dependent on the skill of the examiner, a basic level of competence with the ultrasound examination of the eye should be the goal of every ophthalmologist who manages traumatized eyes.

SUMMARY

Plain film radiography, CT, MRI, and ultrasonography are all methods used to image the ocular and adnexal structures in the evaluation of trauma. Although CT is the best and standard method of evaluating the orbital fractures and aids in the detection of orbital and ocular FBs, both MRI and ultrasonography play supporting roles. In instances of blunt trauma to the globe, however, the roles are reversed: ultrasonography becomes much more important as a diagnostic tool, and radiographic evaluation and MRI play minor roles in the detection and management of the ocular pathology.

REFERENCES

1. Weber AL. Imaging techniques and normal radiographic anatomy. In: Albert DM, ed. *Principles and Practice of Ophthalmology.* Vol 5. Philadelphia, Pa: WB Saunders Company; 1994: 3505–3510.

2. Moseley L. The orbit and eye. In: Sutton D, ed. *A Textbook of Radiology and Imaging*. Vol 2. London, England: Churchill Livingstone; 1993: 1287–1309.

3. Wiesen EJ, Miraldi F. Imaging principles in computed tomography. In: Haaga JR, ed. *Computed Tomography and Magnetic Resonance Imaging of the Whole Body.* Vol 1. St. Louis, Mo: Mosby; 1994: 3–25.

4. Chacko JG, Figueroa RE, Johnson MH, Marcus DM, Brooks SE. Detection and localization of steel intraocular foreign bodies using computed tomography: A comparison of helical and conventional axial scanning. *Ophthalmology.* 1997;104:319–323.

5. Lakits A, Prokesch R, Scholda C, Bankier A, Weninger F, Imhof H. Multiplanar imaging in the preoperative assessment of metallic intraocular foreign bodies: Helical computed tomography versus conventional computed tomography. *Ophthalmology.* 1998;105:1679–1685.

6. Berges O. Orbital ultrasonography: Principles and technique. In: Newton TH, ed. *Radiology of the Eye and Orbit.* New York, NY: Raven Press; 1990: 6.1–6.20.

7. Pavlin C, Harasiewicz K, Sherar M, Foster I F. Clinical use of ultrasound biomicroscopy. *Ophthalmology.* 1991;98:287–295.

8. Pavlin C, Sherar M, Foster F. Subsurface ultrasound microscopic imaging of the intact eye. *Ophthalmology.* 1990;97:244–250.

9. Kramer M, Hart L, Miller JW. Ultrasonography in the management of penetrating ocular trauma [review]. *Int Ophthalmol Clin*. 1995 Winter;35(1):181–192.

10. Deramo VA, Shah GK, Baumal CR, Fineman MS, Correa ZM, Benson WE. Ultrasound biomicroscopy as a tool for detecting and localizing occult foreign bodies after ocular trauma. *Ophthalmology.* 1999;106:301–305.

11. Gunenc U, Maden A, Kaynak S, Pirnar T. Magnetic resonance imaging and computed tomography in the detection and localization of intraocular foreign bodies. *Doe Ophthalmol.* 1992;81:369–378.

12. Kadir S, Aronow S, Davis KR. The use of computerized tomography in the detection of intraorbital foreign bodies. *Comput Tomogr.* 1977;1:151–156.

13. Grove AS Jr. Computed tomography in the management of orbital trauma. *Ophthalmology.* 1982;89:433–440.

14. Zinreich SJ, Miller NR, Aguayo JB, Quinn C, Hadfield R, Rosenbaum A. Computed tomographic three-dimensional localization and compositional evaluation of intraocular and orbital foreign bodies. *Arch Ophthalmol.* 1986;104:1477–1482.

15. LoBue TD, Deutsch TA, Lobick J, Turner DA. Detection and localization of nonmetallic intraocular foreign bodies by magnetic resonance imaging. *Arch Ophthalmol.* 1988;106:260–261.

16 Nasr AM, Barret GH, Fleming JC, Al-Hussain HM, Karcioglu ZA. Penetrating orbital injury with organic foreign bodies. *Ophthalmology.* 1999;106:523–532.

17. Williamson TH, Smith FW, Forrester JV. Magnetic resonance imaging of intraocular foreign bodies. *Br J Ophthalmol.* 1989;73:555–558.

18. Kulshrestha M, Mission G. Magnetic resonance imaging and the dangers of orbital foreign bodies. *Br J Ophthalmol.* 1995;79:1149.